Journal of Marine Science and Technology

Volume 28 | Issue 4 Article 2

ANALYSIS THE KEELUNG HARBOR HYDRODYNAMIC ENVIRONMENT FOR THE SAFETY OF NAVIGATION

Hsing-Yu Wang
Center for General Education, Tzu Chi University, Hualien, Taiwan (R.O.C).

Dong-Taur Su
Department of Shipping Technology, National Kaohsiung University of Science and Technology, Kaohsiung, Taiwan (R.O.C).

Sung-Shan Hsiao
Department of Harbor and River Engineering, National Taiwan Ocean University, Center of Excellence for Ocean Engineering, Keelung, Taiwan (R.O.C)., sshsiao@mail.ntou.edu.tw

Recommended Citation

Wang, Hsing-Yu; Su, Dong-Taur; and Hsiao, Sung-Shan (2020) "ANALYSIS THE KEELUNG HARBOR HYDRODYNAMIC ENVIRONMENT FOR THE SAFETY OF NAVIGATION," *Journal of Marine Science and Technology*: Vol. 28: Iss. 4, Article 2.
DOI: 10.6119/JMST.202008_28(4).0002
Available at: https://jmstt.ntou.edu.tw/journal/vol28/iss4/2

Journal of Marine Science and Technology, Vol. 28, No. 4, pp. 237-248 (2020)
DOI: 10.6119/JMST.202008_28(4).0002

ANALYSIS THE KEELUNG HARBOR HYDRODYNAMIC ENVIRONMENT FOR THE SAFETY OF NAVIGATION

Hsing-Yu Wang[1], Dong-Taur Su[2], and Sung-Shan Hsiao[3]

Key words: Keelung Harbor; harbor entrance; inbound fairway.

ABSTRACT

In this study, we simulated the hydrodynamics of the waters near the Keelung Harbor entrance and fairway before and after harbor expansion. The simulation results are used to discuss the impact of changes in the current characteristic on the inbound vessels. With reference to the fairway planning of Keelung Harbor, the simulation results before the expansion show that the current velocity with inbound fairway during the flood tide ranges from 0.08 to 1.03 m/s. Current direction was affected by the east breakwater, and a circulation occurs near the harbor entrance. After the expansion, during the flood tide, counterclockwise circulations occur near the east breakwater. For the flood tide, current velocity ranges from 0.02 to 0.65 m/s, and during the ebb tide, the current flows to the northeast, and the current velocity ranges on the inbound fairway between 0.07 and 1.22 m/s. Comparing the data on the inbound fairway before and after expansion, the current velocity at the harbor entrance increases. After passing the existing east breakwater for an additional 400 m, the current velocity at the harbor entrance is greatly reduced. Through the calculation results of this study, the necessary conditions for the safety of inbound navigation are provided to avoid the deflection caused by difference in the current at the bow and stern and the resulting improper handling.

I. INTRODUCTION

The Port of Keelung is an important harbor in northern Taiwan. It has been developed for more than 130 years. According to statistics from Taiwan International Ports Corporation, LTD. on the number of entry vessels and inbound cargo tonnage at international commercial ports in Taiwan, the total number of entry vessels (less than 1,000 to 60,000 gross tons) at the Port of Keelung from 2012 to 2019 was 24,450, less than the ports of Kaohsiung and Taichung. However, the total number of containers handled at the Port of Keelung (6,350,752 Twenty-foot Equivalent Unit (TEU)) was only less than the Port of Kaohsiung (40,576,696 TEU). As the Port of Keelung is a harbor built using the natural valley terrain, the development of port capacity has reached its limit, and because of the rise of new ports in the surrounding countries and other factors, the total traffic of the Port of Keelung has shown a significant decline. In recent years, in order to enhance competitiveness, the Port of Keelung has begun to transform into a harbor, combining tourism and entertainment, and is planned as the cruise's home port. According to statistics on the number of international passengers between 2012 and 2019, the number of liners and irregular international cruises calling at the Port of Keelung reached 3,323, which is the highest in Taiwan. The overall data show that the total number of different types of vessels that entered and departed the Port of Keelung was 27,773, indicating that the Port of Keelung is a harbor with heavy maritime traffic in Taiwan. Additionally, the Port of Keelung extended the east breakwater by 200 m on the side of the sea in 2008 to maintain marine transportation and enhance the service capacity of the cruise's home port. The purpose of extending the breakwater was to improve the static stability of the water area of the wharf adjacent to the fairway and the maneuvering basin during the winter monsoon and typhoon. However, changes in the structure of the harbor may affect regional changes in water flow. After the expansion of the east breakwater in the Port of Keelung was completed, Acoustic Doppler Current Profiler (ADCP) and floating buoy system was used (Hsiao et al., 2011) to measure on-site currents. The observation results show that during the flood tide in summer, the path line of the floating buoy placed near the east breakwater is of counter-clockwise rotation. Kao et al. (2010) used numerical models to calculate the current pattern changes before and after the expansion of the east breakwater of the Port of Keelung. The simulation results show the current pattern near the harbor entrance channel was affected by

Paper submitted 02/12/20; revised 03/19/20; accepted 04/16/20. Corresponding Author: Sung-Shan Hsiao (E-mail: sshsiao@mail.ntou.edu.tw)
[1] Center for General Education, Tzu Chi University, Hualien, Taiwan (R.O.C).
[2] Department of Shipping Technology, National Kaohsiung University of Science and Technology, Kaohsiung, Taiwan (R.O.C).
[3] Department of Harbor and River Engineering, National Taiwan Ocean University, Center of Excellence for Ocean Engineering, Keelung, Taiwan (R.O.C).

the extension of the breakwater by 200 m; the current direction changed significantly, and the velocity of the vertical shoreline direction increased. Yuan et al. (2011) also conducted a safety assessment of the entry of large vessels into the port based on the marine environment after the expansion of the east breakwater.

With the development of the government's energy policy, the Hsieh-Ho Power Plant on the west side of Keelung Harbor is expected to be expanded outside the west breakwater, as well as the sea reclamation works, and the power generating units will be converted into natural gas generating units. In order to provide better harbor tranquility for Liquefied Natural Gas (LNG) carriers, the east breakwater with a water depth of about 40 m is planned to continue to extend 400 m to a depth of about 50 m. However, large-scale port expansion projects should once again affect the hydrodynamic characteristics of the area. Tsai et al. (2010) and Li et al. (2010) carried out a numerical simulation of Keelung's sea area for the ocean current energy generation project. The results of the simulation showed that circulation current occurred at the location of Keelung Harbor's expected expansion. Chang et al. (2013) conducted harmonic analysis through long-term monitoring of tidal and current data. The calculation results showed that in addition to the periodic tidal component, the Port of Keelung also has an average velocity of 4.46 cm/s (eastward) and a permanent current of 0.13 cm/s (eastward), and the east to west current is much faster than the north to south. Fang et al. (2018), through the numerical calculations of simulated sea reclamation works and east breakwater extension of 400 m, showed that during the flood tide, the 400 m extension of the breakwater near the harbor entrance causes circulation problems, but the circulation dissipates as the ebb tide velocity increases and the current direction changes. As maritime safety is the major goal of vessel navigation, the ship handling is mainly composed of people, vessels, and the natural environment. The pilot must master and process a large amount of information to maintain or change the state of the vessel's movement and achieve the intended maneuvering purpose. The Port of Keelung is restricted by the geographical environment, and obviously affected by the northeast monsoon. Yang and Liu (2005), Tsou (2019), and Nieh et al. (2019) discussed the issue of vessels entering the Port of Keelung in winter. If the Keelung Harbor expands in the future, it will inevitably cause changes in the current near the fairway and affect the navigation vessels (Armstrong, 2019; Rowe, 2000).

Although ship handling is an applied science subject, the seafarers (such as the pilots) formerly rely on the inheritance of experience to control the movement of ships. Mastering the marine information of vessels entering and leaving the fairway can enhance the safety of navigation, but facing changes in the marine environment caused by the expansion of the harbor, in the future we should fully consider the impact of the marine environment on vessel maneuvering and develop a reasonable ship maneuver plan to cope with the complex environment. In this study, we using a hydrodynamic model that takes into account tidal effects and wave progression, and use winter conditions to simulate the hydrodynamics of the waters near the harbor entrance and fairway before and after Keelung Harbor expansion. The simulation results are used to discuss the impact of changes in the current environment on inbound vessels before and after the expansion. Through the calculation results of this study, the necessary conditions for the safety of inbound navigation are provided to avoid the deflection caused by the difference in the current of the bow and stern and the resulting improper maneuvering.

II. MODEL SETUP AND SIMULATION

In order to understand the influence of the hydrodynamic characteristics before and after the expansion of Keelung Harbor on the vessel's entry and underway, a hydrodynamic model including both wave and tidal characteristics was used for calculation (Chiang et al., 2011; Chiang and Hsiao, 2011; Wang et al., 2018).

2.1 Wave Model

In this study, calculation of wave pattern was carried out by using the mild slope equation of the current effect (Kirby, 1983):

$$\frac{D^2\varphi}{Dt^2}+\left(\nabla\cdot\overline{U}\right)\frac{D\varphi}{Dt}-\nabla\cdot\left(CC_g\nabla\varphi\right)+\left(\sigma^2-k^2CC_g\right)\varphi=0 \qquad (1)$$

where $\overline{U}$ is the ambient current, ∇ is the horizontal gradient operator, φ is the two dimensional velocity potential, k is the wave number, C and C_g are the phase and group speed of the waves, σ is the dispersion relation given by $\sigma^2 = gk\tanh kh$. Under the assumption of irrotational field, single-frequency linear surface waves, the potential energy of a wave can be expressed as follows:

$$\varphi\left(\bar{x},\bar{y},z,t\right)=f\left(z,h\right)\varphi\left(\bar{x},\bar{y},t\right) \qquad (2)$$

where $f\left(z,h\right)=\dfrac{\cosh\left[k\left(h+z\right)\right]}{\cosh kh}$.

In a single periodic harmonic motion, Equation (2) can be rewritten as follows:

$$\varphi\left(\bar{x},\bar{y},t\right)=\mathrm{Re}\left\{ae^{is}e^{i\omega t}\right\} \qquad (3)$$

The following expression can be obtained by substituting Equation (3) into Equation (1) for the real part and imaginary part:
Real part:

$$\frac{1}{aCC_g}\left\{\left(\vec{U}\cdot\nabla a\right)\left[\left(\vec{U}\cdot\nabla\right)+\left(\nabla\cdot\vec{U}\right)\right]\right\} -\frac{1}{a}\left[\nabla^2 a+\frac{1}{CC_g}\left(\nabla CC_g\cdot\nabla a\right)\right]-k^2+\left|\nabla s\right|^2=0 \tag{4}$$

Imaginary part:

$$\nabla\cdot\left[a^2\sigma\left(U+C_g\right)\right]=0 \tag{5}$$

Equations (4) and (5) are the equations of motion for wave interaction before breaking waves. When the current velocity U is known, it solves the system of linear equations in two unknown parabolic simultaneous equations and obtains the amplitude $a(x,y)$ and the wave number $|\nabla s|$. When $\vec{U}=0$, Equations (4) and (5) become:
Real part:

$$\frac{1}{a}\left\{\frac{\partial^2 a}{\partial x^2}+\frac{\partial^2 a}{\partial y^2}+\frac{1}{CC_g}\left[\nabla a\cdot\nabla\left(CC_g\right)\right]\right\}+k^2-\left|\nabla s\right|=0 \tag{6}$$

Imaginary part:

$$\nabla\cdot\left[a^2CC_g\nabla s\right]=0 \tag{7}$$

In addition, energy is dissipated in the surf zone, and the energy expression of Equation (5) must be modified. Based on the energy flux theory, ignore the effect of bottom friction (Mizuguchi, 1980):

$$\frac{d\left(EC_g\right)}{dx}=-\varepsilon,\quad \varepsilon=\frac{1}{2}\rho V_e\left(kH_B\right)^2,\quad V_e=V_{eB}\left(\frac{H_B/2-c'h_B}{\gamma' h_B}\right)^m ,\quad V_{eB}=\frac{5S_B g}{8k_B\rho}\frac{1}{\sqrt{1-C_0}},\quad S_B=\frac{\tan\beta}{1+\frac{3r^2}{2}} \tag{8}$$

where c' is the ratio of the radiation to the water depth of the recovery zone. According to Mizuguchi (1980), $c'=0.17$ when the wave recovery zone is not obvious in a gentle slope.

In the area of wave–current interaction, the energy dissipated by the nearshore current within the surf zone is small and negligible, so the energy amplitude expression according to Equation (8) can be expressed as follows:

$$\nabla\cdot\left[\frac{E}{\sigma}\left(\vec{U}+C_g\right)\right]= -\frac{5}{16}\frac{\rho g^2 k_B}{\sigma^2}\frac{\tan\beta}{1+\frac{3r'^2}{2}}\frac{1}{\sqrt{1-C_0}}\sqrt{\frac{H_B/2-c'h_B}{r'h_B}}\left(H_B\right)^2 \tag{9}$$

With Equation (6), the energy in the surf zone is expressed, and Equation (9) is modified as follows Equation (10).

$$\nabla\cdot\left[a^2\sigma\left(\vec{U}+C_g\right)\right]=\nabla\cdot\left[\frac{2g}{\rho}\frac{E}{\sigma}\left(\vec{U}+C_g\right)\right] =-\frac{5}{8}\frac{g^2k_B}{\sigma}\frac{\tan\beta}{1+\frac{3r'^2}{2}}\frac{1}{\sqrt{1-\frac{c'}{r'}}}\sqrt{\frac{H_B/2-c'h_B}{r'h_B}}\left(H_B\right)^2 \tag{10}$$

In Equations (8)–(10), the subscript B indicates the value at the surf zone. Because the phase function of ϕ is $x\left(\vec{x},t\right)=s\left(\vec{x}\right)-\omega t$, the wave number obtained from the deformed mild slope equation can be expressed as follows:

$$\vec{k}=\nabla x=\nabla s \tag{11}$$

To obtain $|\nabla s|$ from Equations (4), (5), or (10), it is necessary to know the direction of the wave. There are only two equations to solve a, $|\nabla s|$, θ. The linearity of the wave phase function gradient is assumed to be irrotational by Equation (12), and the convergence conditions of wave model is given by Equation (13).

$$\begin{aligned}&\nabla\times\left(\nabla s\right)=0\\&\nabla s=\left|\nabla s\right|\cos\theta\vec{i}+\left|\nabla s\right|\sin\theta\vec{j}\\&\frac{\partial}{\partial x}\left(\left|\nabla s\right|\sin\theta\right)-\frac{\partial}{\partial y}\left(\left|\nabla s\right|\cos\theta\right)=0\end{aligned} \tag{12}$$

$$\begin{aligned}&\left|H_{now}-H_{old}\right|\le\varepsilon_H\left(H_{now}\right),\quad \varepsilon_H=0.001\\&\left|H_{1now}-H_{1old}\right|\le\varepsilon_k\left(H_{1now}\right),\quad \varepsilon_k=0.001\\&\left|H_{2now}-H_{2old}\right|\le\varepsilon_k\left(H_{2now}\right),\quad \varepsilon_k=0.001\end{aligned} \tag{13}$$

2.2 Hydrodynamic Model

In this study, the tidal effect is caused by the tide, which is added to the hydrodynamic model. In addition, the tide is regarded as a long wave, and the Coriolis force effect of the earth's rotation is also considered. The governing equations of the hydrodynamic model are as follows:
Continuity equation:

$$\frac{\partial\eta}{\partial t}+\frac{\partial}{\partial x}\left[U\left(h+\eta\right)\right]+\frac{\partial}{\partial y}\left[V\left(h+\eta\right)\right]=0 \tag{14}$$

Momentum equations:

$$\frac{\partial U}{\partial t}+U\frac{\partial U}{\partial x}+V\frac{\partial U}{\partial y}=fV-g\frac{\partial\eta}{\partial x}+\frac{1}{\rho}\left(\frac{\partial\tau_{xx}}{\partial x}+\frac{\partial\tau_{yx}}{\partial y}\right) +\frac{1}{\rho\left(h+\eta\right)}\left(\tau_{sx}-\tau_{bx}\right)-\frac{1}{\rho\left(h+\eta\right)}\left(\frac{\partial S_{xx}}{\partial x}+\frac{\partial S_{yx}}{\partial y}\right) \tag{15}$$

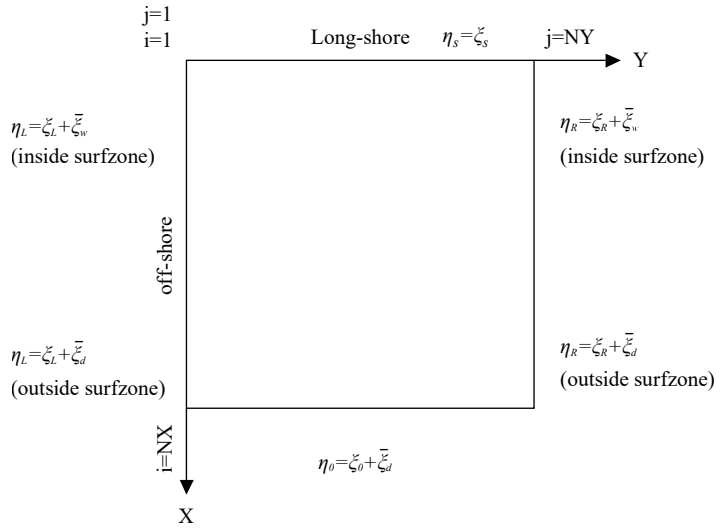

Figure 1. Hydrodynamic model boundary condition diagram

$$\frac{\partial V}{\partial t}+U\frac{\partial V}{\partial x}+V\frac{\partial V}{\partial y}=fV-g\frac{\partial \eta}{\partial y}+\frac{1}{\rho}\left(\frac{\partial \tau_{xy}}{\partial x}+\frac{\partial \tau_{yy}}{\partial y}\right)+\frac{1}{\rho(h+\eta)}\left(\tau_{sy}-\tau_{by}\right)-\frac{1}{\rho(h+\eta)}\left(\frac{\partial S_{xy}}{\partial x}+\frac{\partial S_{yy}}{\partial y}\right) \tag{16}$$

where η is the water surface elevation, h is the static water depth, U and V are the average velocity components of the water depth in the fixed coordinates of the x and y axes:

$$U=\frac{1}{(h+\eta)}\int_{-h}^{\eta}udz,\quad V=\frac{1}{(h+\eta)}\int_{-h}^{\eta}vdz \tag{17}$$

Shear stress τ_{xx}, τ_{xy}, τ_{yx}, τ_{yy} includes viscous stress caused by fluid viscosity and Reynolds stress caused by turbulent effects. Because the value of viscous stress compared with Reynolds stress is very small, viscous stress is ignored generally, and only Reynolds stress is considered to represent the momentum exchange between fluids:

$$\begin{aligned}\tau_{xx}&=\rho E_v\frac{\partial U}{\partial x},\quad \tau_{xy}=\rho E_v\frac{\partial U}{\partial y},\\ \tau_{yx}&=\rho E_v\frac{\partial V}{\partial x},\quad \tau_{yy}=\rho E_v\frac{\partial V}{\partial y},\end{aligned} \tag{18}$$

The vortex viscosity coefficient E_v is obtained from the semi-empirical formula of the Prandtl mixing length theory (Falconer, 1980):

$$E_v=\frac{k_v\sqrt{g}\,(d+h)\sqrt{U^2+V^2}}{6C_c} \tag{19}$$

The sea surface wind shear components τ_{sx} and τ_{sy} are the components of the sea surface wind shear in the x and y directions; refer to Dean and Dalrymple (1984):

$$\tau_{sx}=\rho k_w W^2\cos a;\quad \tau_{sy}=\rho k_w W^2\sin a \tag{20}$$

$$k_w=\begin{cases}1.2\times10^{-5} & ,\ W\le W_c\\ 1.2\times10^{-6}+2.25\times10^{-6}\left[1-\dfrac{W_c}{W}\right]^2 & ,\ W>W_c\end{cases} \tag{21}$$

The bottom friction stress τ_{bx} and τ_{by} are the components in the x and y directions (Ponce and Yabusaki, 1981):

$$\tau_{bx}=\rho E_r U\sqrt{U^2+V^2};\quad \tau_{by}=\rho E_r V\sqrt{U^2+V^2} \tag{22}$$

where the coefficient of the bottom friction $F_r=g/C_c^2$.

The radiation stress S_{xx}, S_{xy}, S_{yx}, S_{yy} is the main factor causing longshore current, which is expressed by the linear wave theory as follows (Longuet-Higgins and Stewart, 1964):

$$\begin{bmatrix}S_{xx} & S_{xy}\\ S_{yx} & S_{yy}\end{bmatrix}=\overline{E}\begin{bmatrix}n\left(1+\cos^2\theta\right)-\dfrac{1}{2} & \left(\dfrac{n}{2}\right)\sin(2\theta)\\ \left(\dfrac{n}{2}\right)\sin(2\theta) & n\left(1+\sin^2\theta\right)-\dfrac{1}{2}\end{bmatrix} \tag{23}$$

where $\overline{E}$ is the total wave energy per unit time and area of section. Under the airy wave theory:

$$\overline{E}=\frac{\rho gH^2}{8} \tag{24}$$

Table 1. Calculation conditions for the hydrodynamic model.

Item	Model setup
Area	5 × 6 km
Grid size	$\Delta x = \Delta y = 25m$
Number of grid points	200 × 240
Time step	$\Delta t = 2\sec$
Time scale	1.0
Wave condition	2.5 m; 8.0 sec; North-northeast (NNE)

The boundary conditions of the hydrodynamic model are shown in Figure 1. The water level change includes the level rise and fall caused by waves and tides.

Tide is a sine function changing from right to left, T_L is the time difference when the tide reaches the left and right boundaries, and T_{start} is the phase difference:

Left boundary:

$$\eta_L = A_L^t \sin\left[\frac{2\pi}{T_t}\left(t + T_t + T_{start}\right)\right], \quad T_t = \frac{L_y}{\sqrt{gh_{Max}}} \tag{25}$$

Right boundary:

$$\eta_R = A_R^t \sin\left[\frac{2\pi}{T_t}\left(t + T_{start}\right)\right] \tag{26}$$

Offshore boundary:

$$\eta_0 = \left[A_R^t + \left(A_L^t - A_R^t\right)\left(\frac{N_y - j}{N_y - 1}\right)\right] \sin\left\{\frac{2\pi}{T_t}\left[t + T_t\left(\frac{N_y - j}{N_y - 1}\right) + T_{start}\right]\right\} \tag{27}$$

The water level $\overline{\xi}$ caused by waves is based on Matushevskiy (1975), ignoring the reflection effect. Equation (28) is the water level descent outside the surf zone, and Equation (29) is the water level uplift in the surf zone:

$$\overline{\xi_d} = -\frac{H^2}{8}\frac{k}{\sinh\left(2kh\right)}\left(\cos\theta\right)^{2/3} \tag{28}$$

$$\frac{d\overline{\xi_u}}{dx} = -K\frac{dh}{dx}, \quad K = \frac{1}{1 + \left(8/3\gamma^2\right)} \tag{29}$$

The left boundary of the velocity is shown in Equation (30), the right boundary is shown in Equation (31), the offshore boundary is shown in Equation (32), and the longshore boundary is shown in Equation (33).

$$U_{j=1} = U_{j=2}, \quad \left(\frac{\partial V}{\partial y}\right)_{j=1} = 0 \tag{30}$$

$$U_{j=NY} = U_{j=NY-1}, \quad \left(\frac{\partial V}{\partial y}\right)_{j=NY} = 0 \tag{31}$$

$$U_{j=NX} = U_{j=NX-1}, \quad \left(\frac{\partial U}{\partial x}\right)_{j=NX} = 0 \tag{32}$$

$$U = 0, \quad V = 0 \tag{33}$$

The stability of the hydrodynamics calculation must satisfy $\Delta t \le 2\Delta s / \sqrt{gh_{Max}}$, where Δs is the grid size. The maximum value of two adjacent time steps is less than the allowable error with Equation (34), and then the calculation of the next time step can be performed.

$$\begin{aligned} &Max\left(\eta_{ij}^{k+1} - \eta_{ij}^{k}\right) \le \varepsilon_\eta \eta_{ij}^{k}, \quad \varepsilon_\eta = 0.0001 \\ &Max\left(U_{ij}^{k+1} - U_{ij}^{k}\right) \le \varepsilon_U U_{ij}^{k}, \quad \varepsilon_U = 0.0001 \\ &Max\left(V_{ij}^{k+1} - V_{ij}^{k}\right) \le \varepsilon_V V_{ij}^{k}, \quad \varepsilon_V = 0.0001 \end{aligned} \tag{34}$$

2.3 Modeling Procedure and Validation

The model was developed by examining the environmental background data, selecting the range to be simulated, and calibrating the tidal model. Field investigation was performed, and data were collected to calculate the required environmental background data using the integrated model. The model calculation area is shown in Figure 2. A numerical topography with a longshore of 5 km and an offshore of 6 km was established around the Port of Keelung. The water depth was established by using the Ministry of Science and Technology's 200 m grid topographic data. The calculation conditions of the numerical model were mainly obtained by the observation station (code X2) shown in Figure 3, and referring to the field observation data of the Harbor and Marine Technology Center. Table 1 lists the configuration settings of the hydrodynamic model. Figure 4 compares the model simulation results with

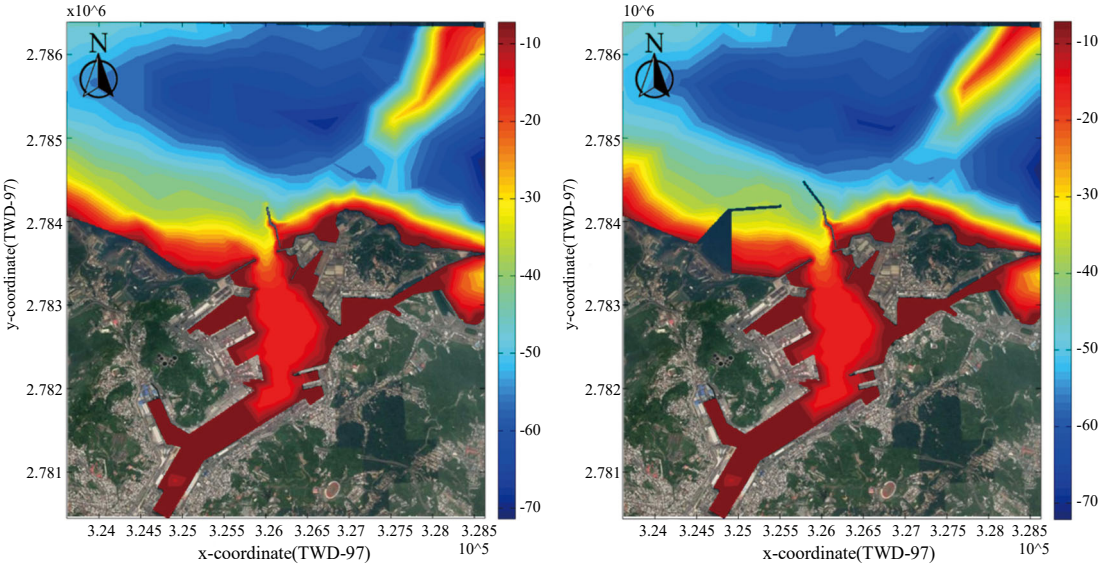

Figure 2. Geographic location and computed domain in the Port of Keelung. (a) Before expansion; (b) after expansion.

Figure 3. Current and Wave observation station (X2) in computed domain.

the current measurement. The calculated current velocity, current direction, and changes in water level were all highly consistent with the measured data. The currents simulated by the model generally flowed parallel to the coastline. Specifically, the current flowed from the east to the west during flood tides and from the west to the east during ebb tides. The results, in accordance with the actual situation, indicate that the model successfully reproduced the characteristics of the current in the sea area adjacent to the Port of Keelung. After the boundary conditions and related parameters adopted by the hydrodynamic model were determined, the model was employed to calculate the hydrodynamic characteristics before and after the Port of Keelung expansion and to discuss the impact of regional current pattern changes on inbound vessels).

III. ANALYSIS OF THE IMPACT OF HYDRODYNAMIC CHANGE ON INBOUND NAVIGATION

3.1 Hydrodynamic Simulation Results

The results of the hydrodynamic simulation are shown in Figures 5 to 7. Figure 5 shows the results of the wave field before and after the expansion. Large changes in wave height

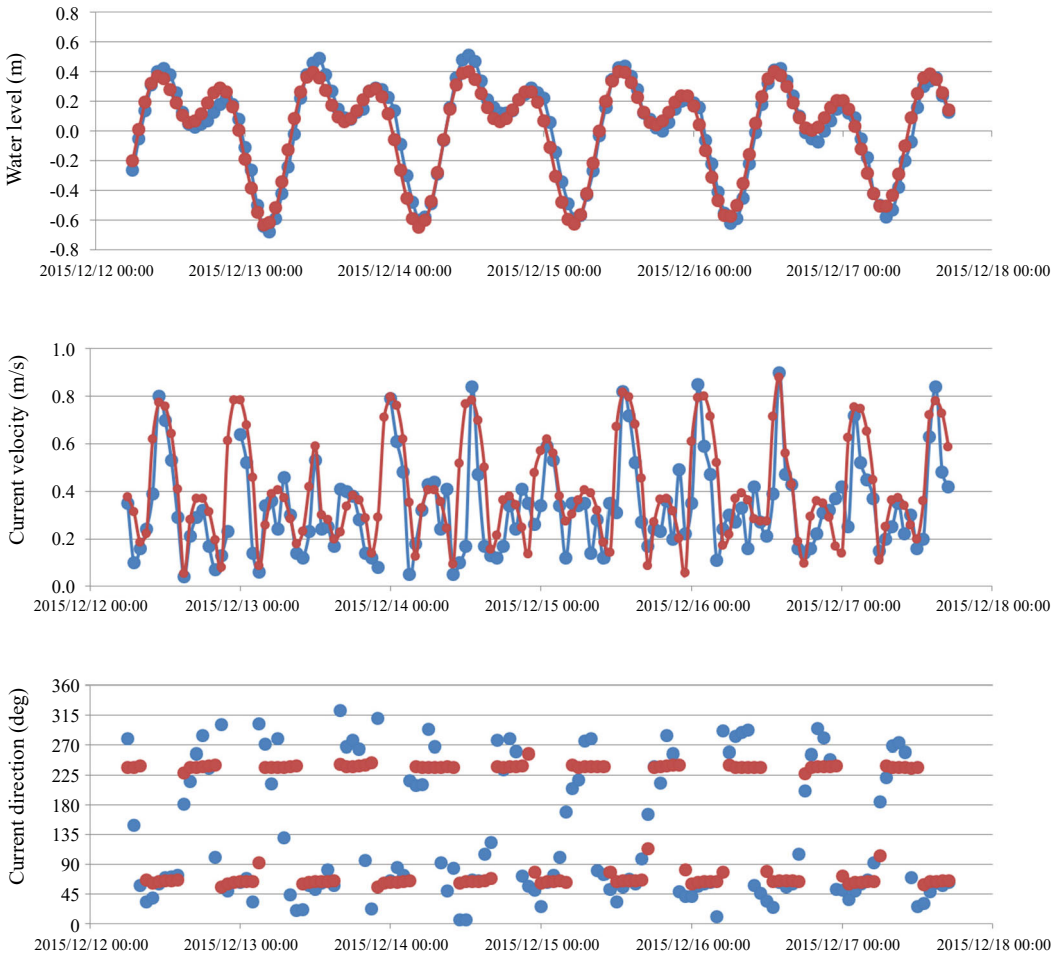

Figure 4. Comparison between the numerical model and the measured data. Blue line, measurement data; red line, simulation results.

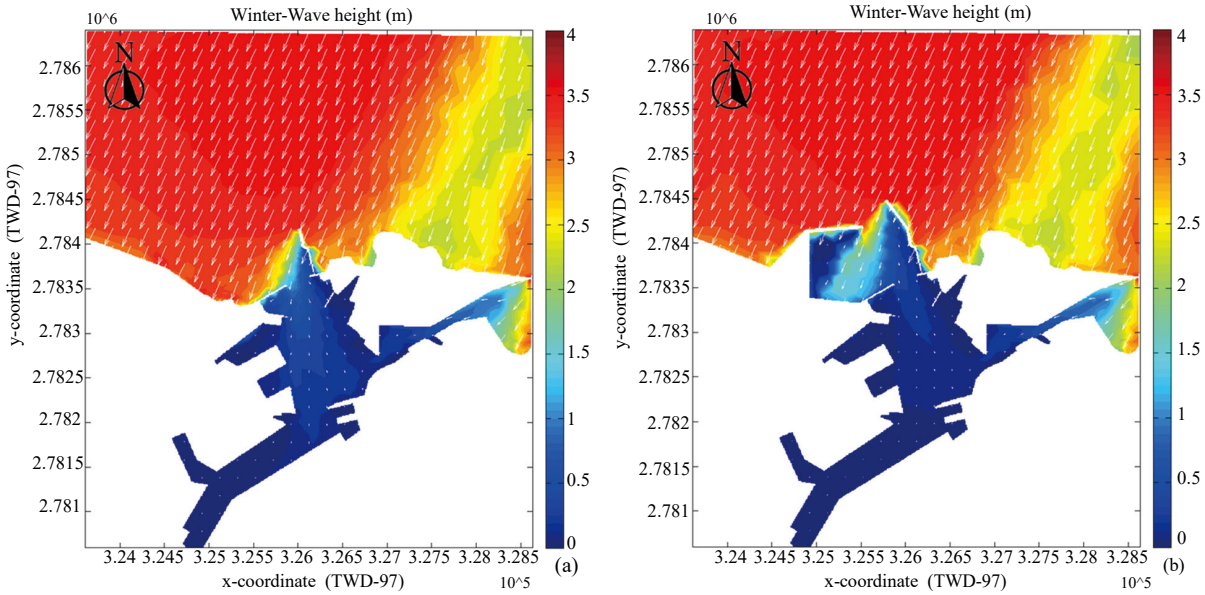

Figure 5. Computed wave distribution of winter waves. (a) Before expansion; (b) after expansion.

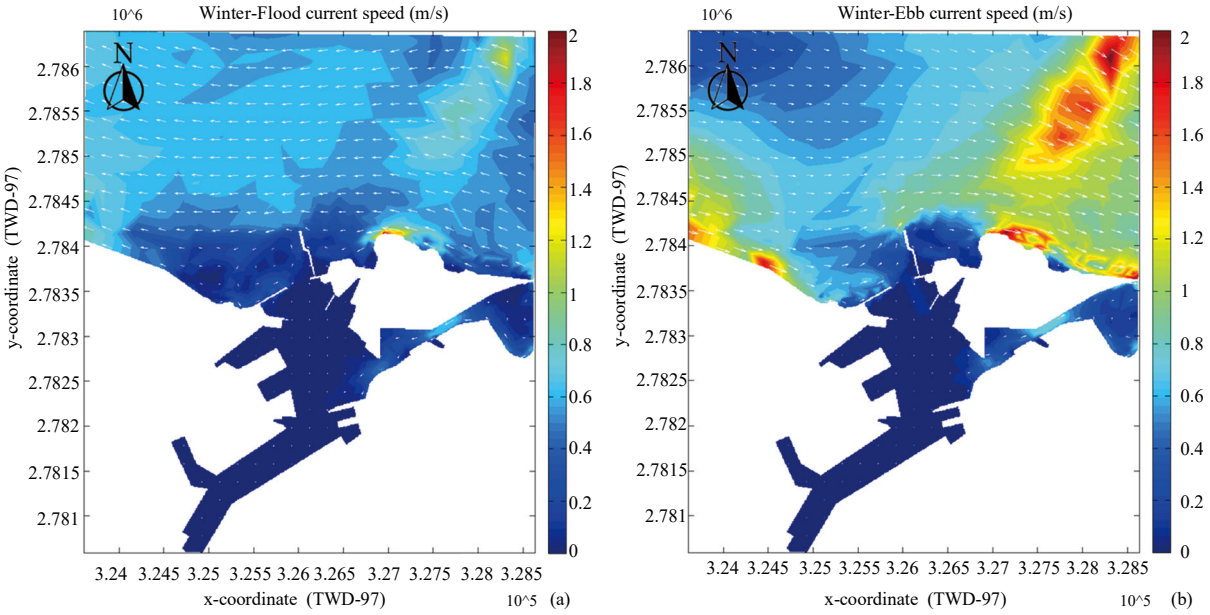

Figure 6. Computed current pattern during flood (a) and ebb (b) tides in the Port of Keelung before expansion.

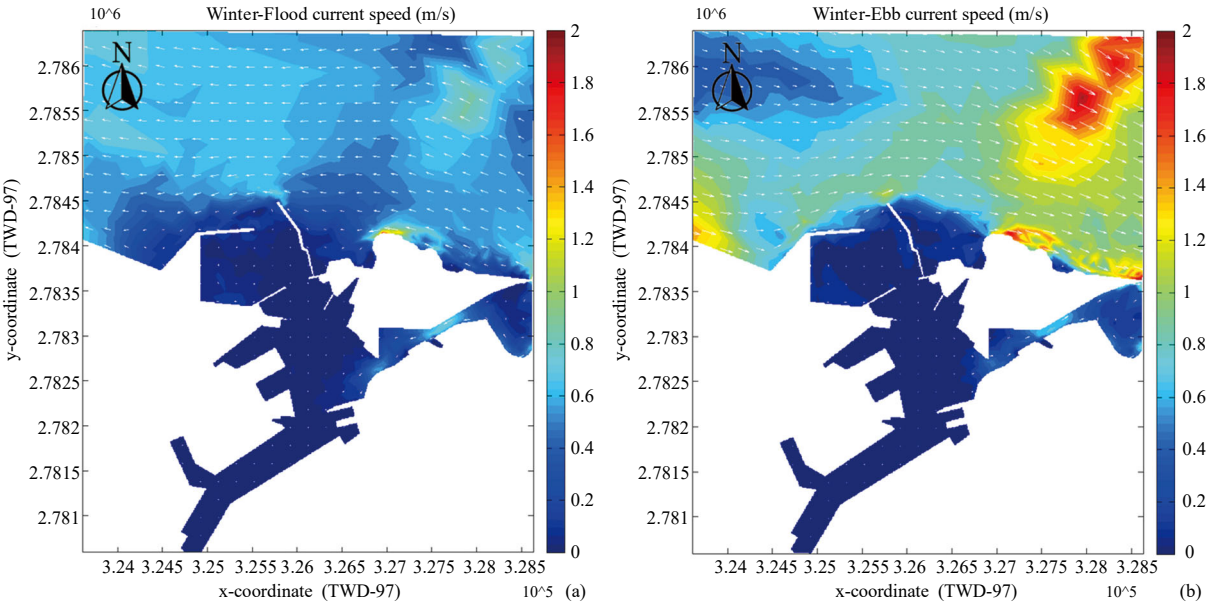

Figure 7. Computed current pattern during flood (a) and ebb (b) tides in the Port of Keelung after expansion

occur in places where the topography changes greatly. Figure 6 to 7 shows the simulation results of the current pattern. The large current velocity occurs near the steep topography and near the breakwater. Because the characteristics of the current in the nearshore mainly reflect the mechanism of tide–wave interaction and the nearshore topographical characteristics, after the expansion of the Hsieh-Ho Power Plant, the local current conditions will change with the topographical characteristics. From the model, it was calculated that the current flows from the east to the west during flood tides and from the west to the east during ebb tides, and the current velocity increases due to the effect of topography between Keelung Island and the Port of Keelung. From the extension of the fairway outside the harbor entrance to the breakwater, the average velocity during the flood tide is about 0.26–0.62 m/s, and the average velocity during the ebb tide is about 0.46–1.03 m/s. The distribution of the current direction shows that due to the influence of the east breakwater, a circulation occurs. In addition, the simulation results after the expansion show that the current pattern in the sea area was affected by the extension of the breakwater. During the flood tide, the anti-clockwise circulation occurred near the east breakwater extending 400 m, with

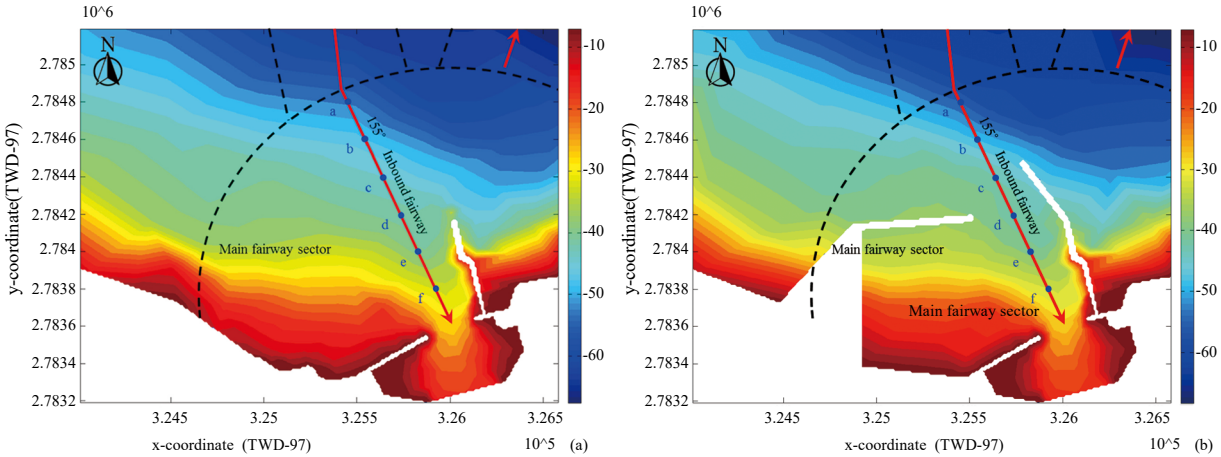

Figure 8. Schematic diagram of data extraction points on inbound fairway. (a) Before expansion; (b) after expansion.

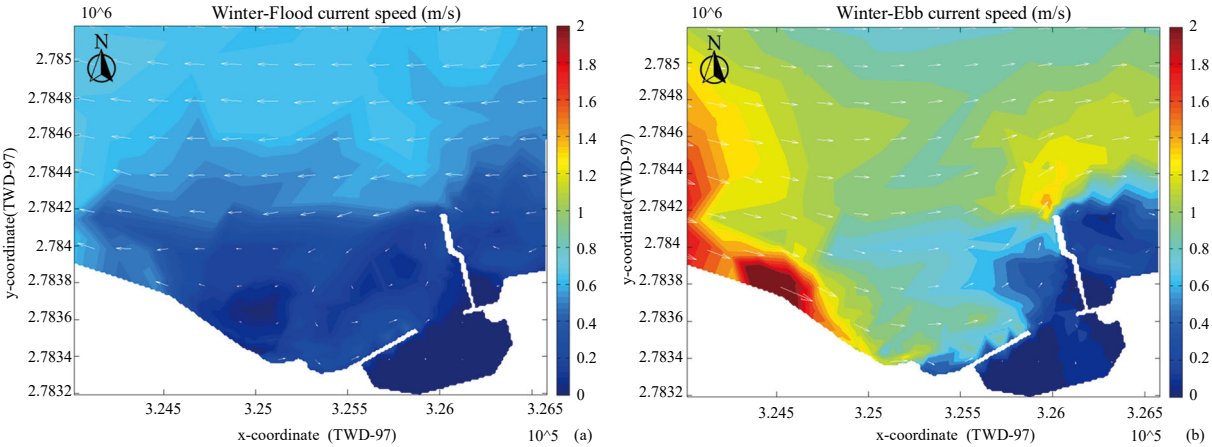

Figure 9. Computed current pattern during flood (a) and ebb (b) tides in the Port of Keelung before expansion

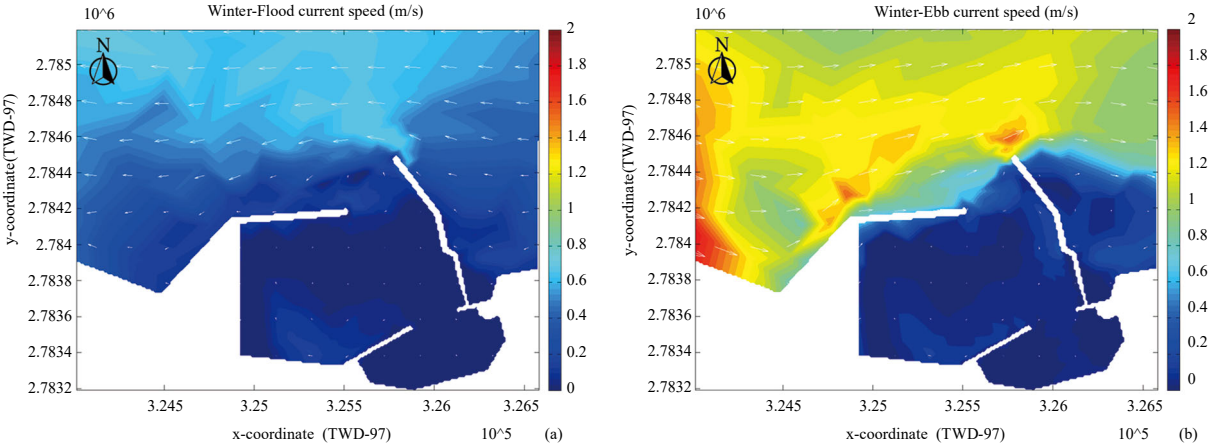

Figure 10. Computed current pattern during flood (a) and ebb (b) tides in the Port of Keelung after expansion.

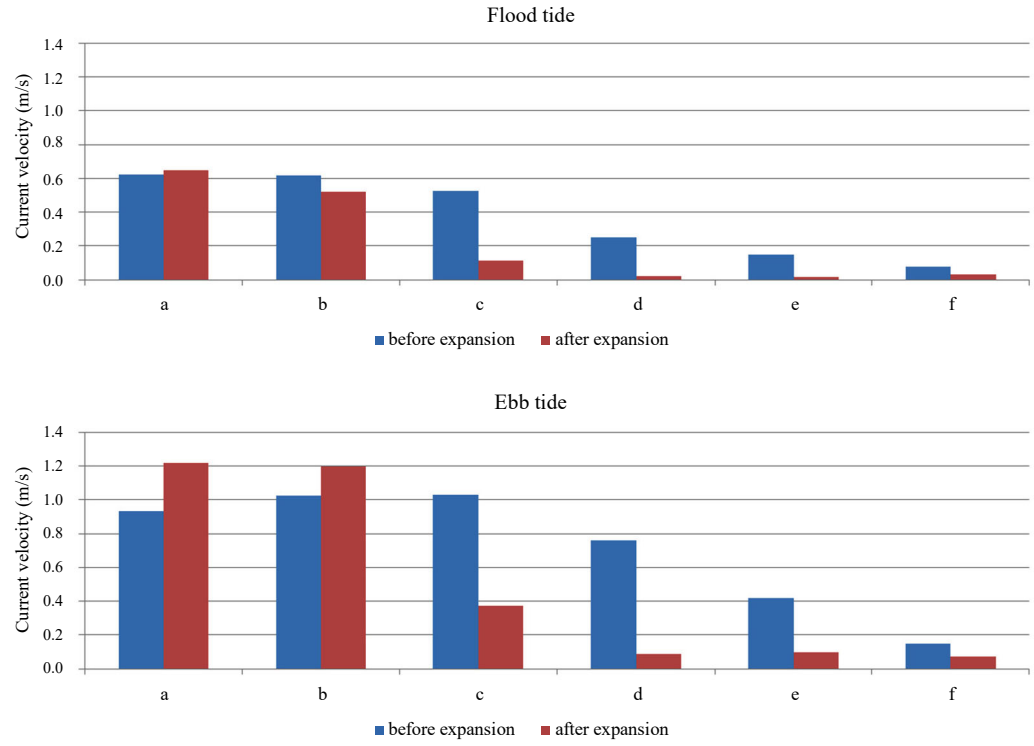

Figure 11. Comparing the current velocity on the inbound fairway before and after the expansion.

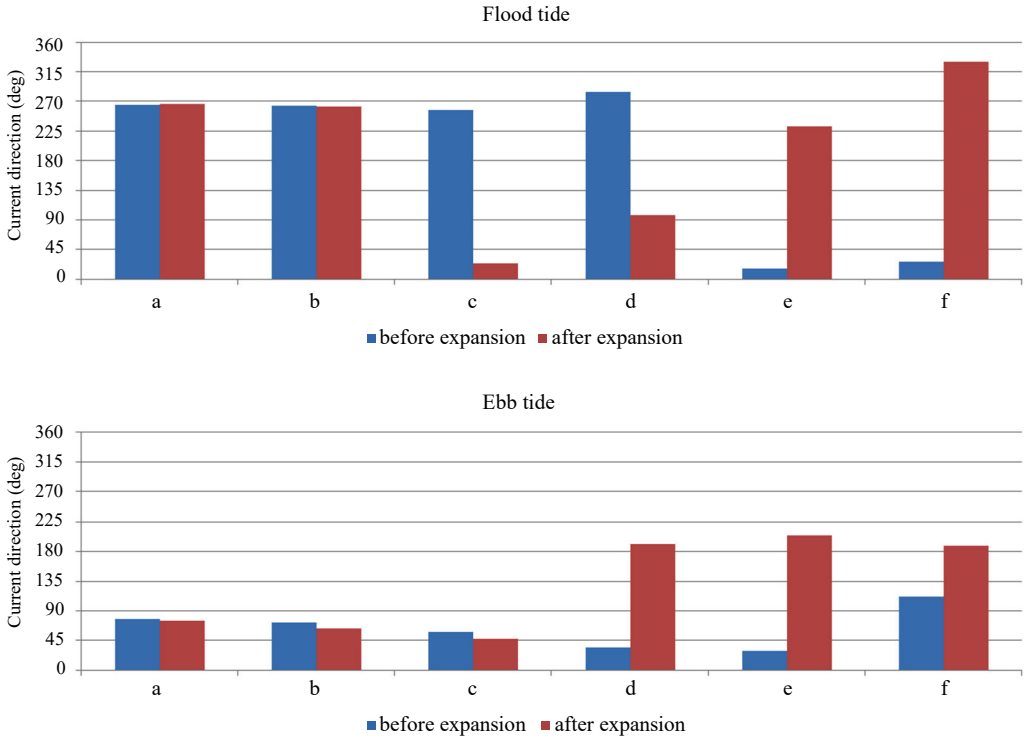

Figure 12. Comparing the current direction on the inbound fairway before and after the expansion.

an average velocity of about 0.31–0.65 m/s. During the ebb tide, the current flowed northeast, with an average velocity of about 0.52–1.22 m/s.

3.2 Hydrodynamic Characteristics at the Inbound Navigation

With reference to the existing fairway planning of Keelung Harbor, we extracted the simulation results of the main fairway sector, shown in Figure 8, and conducted data acquisition and discussion at an interval of 200 m on the inbound fairway. The hydrodynamic simulation results after being captured near the main fairway sector are shown in Figure 9. The simulation results before the expansion show that the current velocity from a to f during the flood tide is within the range of 0.08–0.62 m/s, and the current velocity from a to f during the ebb tide is within the range of 0.15–1.03 m/s. Current direction distribution shows that due to the influence of the east breakwater, a circulation occurs near the shore. The simulation result after the expansion is shown in Figure 10, which is affected by the breakwater after the expansion, resulting in a change in the current pattern. During the flood tide, a counterclockwise circulation occurs near the east breakwater. During the flood tide, the current velocity is within the range of 0.02–0.65 m/s, and during the ebb tide, the current flows to the northeast, and the current velocity is within the range of a to f between 0.07 and 1.22 m/s. Comparing the data collected on the inbound fairway before and after the expansion, as shown in Figures 11 and 12, it can be found that the structure extends to the sea after the expansion. Although there is no difference in the current direction affected by the structure, the current velocity at points a and b increases. After passing the existing east breakwater for an additional 400 m, the current velocity at points c–f is greatly reduced, and the current direction is greatly changed.

In the future, in order to meet the needs of the Hsieh-Ho Power Plant, the Port of Keelung is planned to expand with sea reclamation works. The calculation results based on the measured data in the sea area show that after the expansion, the static stability in the harbor is maintained, but the distribution of the nearby water flow is changed. Because the vessel sails at the harbor entrance of the fairway, it is affected by the cross-current effect of the vessel's maneuvering characteristics, and because the Port of Keelung is located in Northern Taiwan, it is significantly affected by the northeast monsoon. The simulation results of the hydrodynamic environment before and after the expansion can provide considerations for piloting and rudder timing to avoid accidents.

IV. CONCLUSION

With the Port of Keelung as a research subject, in this study, we simulated the current characteristics of the before and after expansion conditions. The coupling effect of waves–currents was considered in this model. The following conclusions can be drawn from the simulation results:

1. Before the expansion of Hsieh-Ho Power Plant, the harbor entrance channel flowed from southwest (SE) to northwest (NW) at flood tide, the average current velocity was 0.26–0.62 m/s, and it had the characteristics of circulation. Circulation dissipated as the ebb tide velocity increased and the current direction changed. The ebb tide flow was from northwest (NW) to southwest (SE), with an average velocity between 0.46 and 1.03 m/s. Because there was no structural influence during ebb tide, the current velocity during ebb tide was faster than flood tide.
2. After the expansion of Hsieh-Ho Power Plant, the tide current is affected by the extension of the east breakwater, and counter-clockwise circulation occurs near the east breakwater head, with an average velocity of about 0.31–0.65 m/s. During the ebb tide, the current flows to the northeast, with an average velocity of about 0.52–1.22 m/s. The circulation near the harbor entrance channel gradually moves northward with the direction of the water flow, and then dissipates as the current direction of the ebb tide changes.
3. Before the expansion, the current velocity decreased from 0.62 to 0.08 m/s between the inbound fairway outside the harbor entrance and the breakwater, and the current velocity was from 0.15 to 1.03 m/s during the ebb tide. The impact of the east breakwater head caused circulation. After the expansion, affected by the 400 m extension of the east breakwater, the flood tide current velocity ranges from 0.02 to 0.65 m/s from the harbor entrance channel to the breakwater, and a counterclockwise circulation occurs at the head of the breakwater. During the ebb tide, it is between 0.07 and 1.22 m/s. After the expansion, the structure extends to the sea, and the structure affects the current velocity near the harbor entrance.
4. The simulation results show that after the expansion of Hsieh-Ho Power Plant, the affected area is roughly in the sheltered area on both sides of the breakwater and near the breakwater head. The current velocity slows down near the west breakwater, the current direction changes significantly, and a circulation occurs between the east and west breakwaters. The hydrodynamic simulation results before and after the expansion through this study can provide a reference for the safety assessment calculations required for ships entering, as well as considerations for piloting and rudder timing assessment.

REFERENCES

Armstrong, M.C. (2019). Practical Ship Handling, The Nautical Mind.

Hsiao, S.-S., H.-M. Fang, L.-M. Chern, H.-Y. Wang and C.-L. Ting (2011). Characteristics of the current pattern near the entrance of Keelung Harbor. Proceedings of the 21st International Offshore and Polar Engineering Conference, 943-948.

Kao, J.-H., J.-F. Lee, C.-C. Liu, Y.-F. Chiu, C.-H. Su and C.-Y. Lee (2010). Flow simulation of keelung harbor with an extension to eastern

breakwater. Proceedings of the 32nd Ocean Engineering Conference in Taiwan, 381-385. (in Chinese)

Tsai, C.-H., D.-J. Doong, Y.-Z. Kehr, H.-W. Li, C.-R. Ho, N.-J. Kuo, S.-J. Huang, Y.-T. Lo and H.-J. Lee (2010). A pilot project on ocean energy generation by tidal currents on the northern coast of Taiwan, OCEANS'10 IEEE SYDNEY.

Yuan, S.-G., C.-C. Tsai and J.-C. Huang (2011). A safety assessing model for a large vessel sailing into Keelung Harbor, Maritime Quarterly 29(3), 19-37. (in Chinese)

Fang, H.-M., C.-C. Wen, H.-Y. Wang, C.-M. Fan and H.-Y. Li (2018). Study on the Diffusion of thermal discharge around the Hsieh-Ho power plant. Proceedings of the 40th Ocean Engineering Conference in Taiwan. (in Chinese)

Chang, H.-K., W.-J Juang and H.-M. Tseng (2013). Comparisons of main components of astronomic tides and tidal currents at seven taiwan ports. Journal of Coastal and Ocean Engineering 13(4), 393-410. (in Chinese)

Li, H.-W., Y.-T. Lo, C.-H. Tsai, N.-J. Kuo, C.-R. Ho, D.-J. Doong, S.-J. Huang, H.-J. Lee and Y.-Z. Kehr (2010). Numerical simulation of tidal current around Keelung Sill off Northern Taiwan, OCEANS'10 IEEE SYDNEY.

Yang, Y.-L. and J.-Z. Liu (2005). Maneuvering of entering and berthing of Keelung Harbor in winter. Journal of Qingdao Ocean Shipping Mariners College 26(4), 42-44. (in Chinese)

Tsou, M.-C. (2019). Big data analytics of safety assessment for a port of entry: A case study in Keelung Harbor. Journal of Engineering for the Maritime Environment 233(4), 1260-1275.

Nieh, C.-Y., M.-C. Lee, J.-C. Huang and H.-C. Kuo (2019). Risk assessment and traffic behaviour evaluation of inbound ships in Keelung Harbour based on AIS data. Journal of Marine Science and Technology 27(4), pp. 311-325.

Rowe, R. W. (2000). THE SHIPHANDLER'S GUIDE for Masters and Navigating Officers, Pilots and Tug Masters, The Nautical Institute.

Chiang, Y.-C., S.-S. Hsiao and M.-C. Lin (2011). A Quasi-3D sediment transport modeling for coastal morphodynamics. Proceedings of the 21st International Offshore and Polar Engineering Conference, 1053-1058.

Chiang, Y.-C. and S.-S. Hsiao (2011). Coastal morphological modeling. Sediment Transport in Aquatic Environments Ch. 10, 203-230.

Wang, H.-Y., H.-M. Fang and S.-S. Hsiao (2018). Morphological characteristics of tidal inlets subject to a short term typhoon event: A case study in Lanyan River estuary. Journal of Marine Science and Technology 26(4), 552-561.

Kirby, J. T. (1983). A parabolic equation for the combined refraction-diffraction of Stokes waves by mildly varying topography. Journal of Fluid Mechanics 136, 453-466.

Mizuguchi, M. (1980). An heuristic model of wave height distribution in surf zone, Proc. 17th Coastal Eng. Conf , ASCE, 278-289.

Falconer, R. A. (1980). Numerical modeling of tidal circulation in harbors. J. Wtrwy., Port, Coast., and Oc. Div., ASCE, 106(1), 31-48.

Dean, R. G. and R. A. Dalrymple (1984). Water Wave Mechanics for Engineers and Scientists, Prentice-Hall, Inc., New Jersey.

Ponce, V. M. and S. B. Yabusaki (1981). Modeling circulation in depth-averaged flow, J. Hydr. Div., ASCE, 107(11), 1501–1518.

Longuet-Higgins, M. S. and R. W. Stewart (1961). The changes in amplitude of short gravity waves on steady non-uniform currents. Journal of Fluid Mechanics 10, 529-549.

Longuet-Higgins, M. S. and R. W. Stewart (1964). Radiation in water waves: a physical discussion with applications. Deep-sea Research 11, 529-563.

Matushevskiy, T. V. (1975). Method of separation of wave induced and turbulent motions in the near-surface layer of the ocean, in On Problems of Ocean Dynamics, 124– 151. (in Russian)